Experimental Characterization of Stall Noise Toward its Modelling

Bertagnolio, Franck; Aagaard Madsen , Helge; Fischer, Andreas; Bak, Christian

Published in:
Proceedings of the 6th International Conference on Wind Turbine Noise

Publication date:
2015

Document Version
Publisher's PDF, also known as Version of record

6th International Conference
on
Wind Turbine Noise
Glasgow 20-23 April 2015

Experimental Characterization of Stall Noise Toward its Modelling

Franck Bertagnolio, DTU Wind Energy, Frederiksborgvej 399, DK-4000 Roskilde, Denmark, E-mail: frba@dtu.dk

Helge Aa. Madsen, DTU Wind Energy, Frederiksborgvej 399, DK-4000 Roskilde, Denmark, E-mail: hama@dtu.dk

Andreas Fischer, DTU Wind Energy, Frederiksborgvej 399, DK-4000 Roskilde, Denmark, E-mail: asfi@dtu.dk

Christian Bak, DTU Wind Energy, Frederiksborgvej 399, DK-4000 Roskilde, Denmark, E-mail: chba@dtu.dk

Summary

Wind tunnel measurements of three different airfoils are investigated using surface pressure microphones flush-mounted on the suction side of the airfoils. In stalled conditions, these microphones can be used to evaluate the convection velocity and the correlation length of the turbulent vortices that are generated in the separated region of the stalled flow. In addition, stall is characterized by the appearance of a spectral hump at relatively low frequencies that can be measured by the microphones located in the separated region. Using appropriate normalization and scaling, a nearly universal model that can represent the behavior of the surface pressure spectra in this low frequency range is devised.

1. Introduction

Among wind turbine noise mechanisms, amplitude modulation has appeared to be a great source of annoyance at neighbouring dwellings. Amplitude modulation may occur through several noise generation mechanisms (see Smith et al. (2012) for a review). One of them originates from the flow over a section of the blade momentarily entering stall yielding to a so-called ‘Other Amplitude Modulation’ mechanism. This phenomenon obviously occurs for stall-regulated wind turbines, explaining why the latter are often perceived as more noisy than pitch-regulated wind turbines in particular at high wind speeds. Nevertheless, it was recently shown by Madsen et al. (2014) that stall is also likely to occur for pitch-regulated turbines at low wind speeds, in which case the wind turbine noise annoyance is maximal since there is less masking effect from the ambient noise created by the wind itself in the surroundings. The mechanism behind the latter occurence of stall can be explained by the fact that pitch-regulated turbine controllers use rotor rotational speed as a target in their control loop

algorithm at low wind speeds. The great inertia of the rotor (typically tens of tons for a modern MW turbine) prevents the wind turbine controller to quickly achieve the desired rotor speed when the wind speed changes too rapidly due to wind gusts or the natural variability of the wind.

Stall over an airfoil occurs when the angle of attack of the inflow relative to the airfoil chord becomes larger than a critical value. In this case, the flow over the airfoil no longer smoothly follows the contour of the airfoil (referred to as 'attached flow') and flow separation occurs on the suction side of the airfoil. This typically yields a turbulent flow region above the suction side that further convects downstream into the wake. This phenomenon is associated with a significant reduction of the airfoil lift and large increase of drag. Different airfoil shapes yield different critical values of the angle of attack and patterns in the occurence of stall. Some airfoils may stall abruptly at some specific angle of attack. Other types of airfoil (typically more cambered ones) experience a more progressive stall for which the flow initially separates in a small region in the vicinity of the trailing edge while the flow remains attached over the main part of the airfoil. Then, the size of this separated region grows as the angle of attack increases, until deep stall is reached when the flow over most of the airfoil chord is no longer attached. For some airfoils, stall separation may initiate at the leading edge typically yielding an abrupt stall, but this case is less frequent and will not be considered in this contribution. Note that the occurence of stall is also influenced by the Reynolds number of the airfoil flow.

As described above, stall is characterized by a turbulent flow, and thereby turbulent vortices developping over the suction side of an airfoil that subsequently convect into the wake of the airfoil. These vortices are necessarily interacting with the surface of the airfoil itself, leaving a footprint in the form of turbulent surface pressure fluctuations, and are consequently generating noise. This mechanism may be denoted as 'self-noise' in the aero-acoustic terminology since the airfoil is itself producing the turbulent vortices which are interacting with the airfoil surface to generate noise.

The final aim of this study is to develop a stall noise model. To formulate such a model, an approach alike to the one followed by Moreau et al. (2009) is proposed. It consists in modelling the effect of the turbulent vortices on the surface as dipole acoustic sources. The model formulation requires the knowledge of the convection velocity of the turbulent surface pressure fluctuations, their length scales and their spectral contents. In contrast to Moreau et al. (2009) who directly make use of surface pressure fluctuations measured on an airfoil placed in a wind tunnel in order to specify these input data, our intent is to develop a semi-empirical model which inputs are based on mean flow quantities and which is not relying on measurements. However, the model physical parameters will be tuned using experimental results.

In this paper, the stall phenomenon is experimentally investigated in a wind tunnel. The turbulent stall vortices are characterized using surface pressure microphones flush-mounted on airfoil sections. The next section describes the experimental set-up and stall is characterized using mean aerodynamic flow quantities in Section 3. In the following two sections, the convection velocity and correlation length of the surface pressure fluctuations are analyzed, respectively. Section 6 deals with the surface pressure spectra and their scaling. The results of this study and future developments are discussed in the last section.

2. Description of Experimental Set-Up

Measurements of three different airfoil sections were conducted in the LM Wind Power wind tunnel in Lunderskov (see Madsen et al. (2010)). Their shapes correspond to the NACA-0015, NACA-63-418 and RISØ-B1-18 airfoil profiles. The airfoil models were equipped with pressure taps and surface pressure microphones.

The pressure taps were connected through a tubing system to a Scanivalve ZOC33/-TCU64Px pressure scanner. Data were recorded by a Scanivalve RAD3200 Remote A/D converter that interfaced the ZOC pressure scanners to a PC. The acquisition system has a sampling frequency of 100 Hz, but only averaged values will be displayed in the following.

The turbulent surface pressure fluctuations were measured with Sennheiser KE 4-211-2 microphones (see Fig. 1(a)) distributed around the section profiles. These microphones have an almost flat response for the frequency range of the spectra considered in this work that makes them suitable for the present analysis. The experimental set-up with the microphone housing has been developed during previous measurement campaigns (see Fischer et al. (2010)). The signals were treated by an amplifier located just beneath the microphones and further acquired by a National Instruments CompactRIO-9052 sampling up to 50 kHz. The microphones were mounted within flushing adaptors, as shown in Figs. 1(a-b), which were then screwed into holes threaded within the section material. The microphones were calibrated in this set-up configuration by Brüel & Kjær (see Guastavino (2010)). The calibration technique consisted in using a headphone which can be actuated with a monotone excitation frequency, the frequency being incrementally varied across the whole spectral range of interest. An accurate Brüel & Kjær probe microphone Type 4182 was used as a reference. This type of probe allows sound pressure measurements in small and awkward places as the probe is terminated with a small diameter tube. The probe is itself calibrated with the above tubing device. The end of the probe tube was taped very close to the flushing adaptor hole and both were confined under the headphone padding to insulate from exterior disturbances. The main findings during the calibration study were that the microphones have a relative flat response up to 12 kHz with deviations below 2dB.

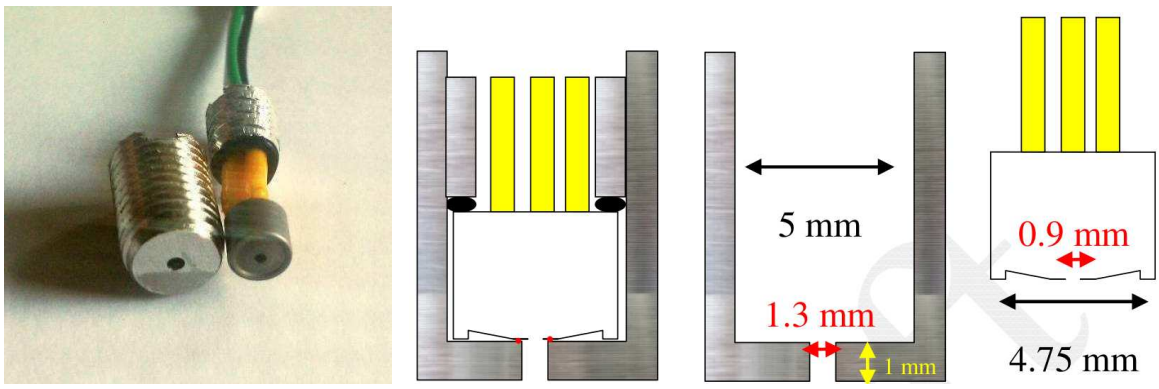

(a) KE 4-211-2 microphone and flushing adaptor

(b) Sketch of microphone mounting

Figure 1: Surface microphones set-up [Pictures courtesy of Brüel & Kjær]

The microphones were distributed around the airfoil sections. However, due to obvious space requirements in order to flush-mount the microphones with their housings, these could not be located very close to the trailing edge. Furthermore, the chordwise distribution of the microphones varies from one airfoil to the other. As a consequence,

the entire stall region is not always covered by the microphones in the following analysis. It is due to the fact that the experiments were mainly designed to monitor the transition location from laminar to turbulent flow in the boundary layer and were not intended for the present study of stall characteristics. In addition, the microphones were distributed at slightly different span locations along the chord in order to avoid the wake created by upstream microphones to disturb the measurements at downstream ones. However, for the present study the slight spanwise off-sets of the different microphones can be neglected in comparison to the relatively large size of the vortical structures of interest.

The measurements were carried out in a clean tunnel with a turbulence intensity around 0.1%. The airfoil sections were tested at various angles of attack and for the following Reynolds numbers $Re = 3, 4, 5$ and 6×10^6 defined as $Re = \rho U_\infty C/\mu$ where ρ is the fluid density, μ its dynamic viscosity, U_∞ is the inflow velocity and C is the airfoil chord.

3. Detection and Characterization of Stall Using Aerodynamic Quantities

As mentioned in the introduction, stall is associated with a decrease of lift. In Figs. 2(a-b-c). The lift coefficient curves are plotted as a function of the angle of attack α for the different airfoils at the Reynolds numbers considered in the experiment. It can be observed that up to a certain angle of attack, lift grows linearly. Then, the slopes of these curves start to decrease indicating the initiation of stall, most probably associated with the appearance of a recirculating flow near the trailing edge. Soon after, the lift starts to decrease indicating the rapid growth of the separated region to larger portions of the airfoils chord.

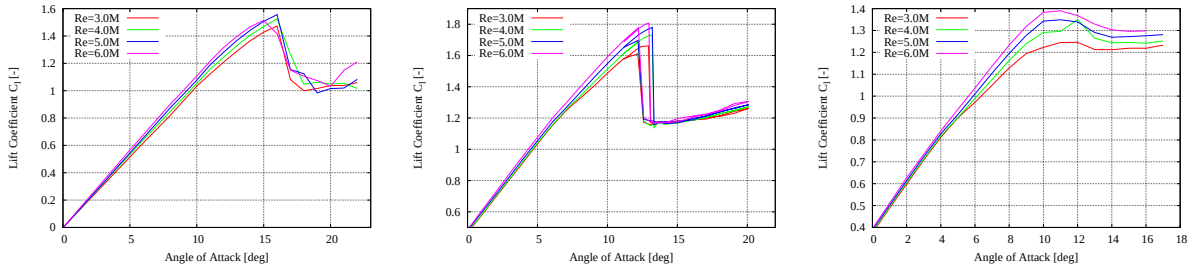

(a) NACA-0015 (b) RISØ-B1-18 (c) NACA-63-418

Figure 2: Polar curves

The above scenario can be observed in more detail looking at the pressure coefficient distributions around the airfoils as displayed in Figs 3(a-b-c). Note that these pressures are measured with the pressure taps and are plotted as differential pressure values relatively to the static atmospheric pressure. Two angles of attack are displayed only: one for which the flow is attached and one for the stalled flow. In these plots, the pressures are averaged over time in order to get stationary values. In contrast to lower angles of attack, pressure coefficient distributions at high angles of attack exhibit a plateau on the suction sides characteristics of stall separation.

4. Stochastic Characterization of Stall through Convection Velocity

The stall phenomenon can be characterized by the flow over an airfoil for which the streamlines no longer follow the contour of the airfoil, but rather separates to form a

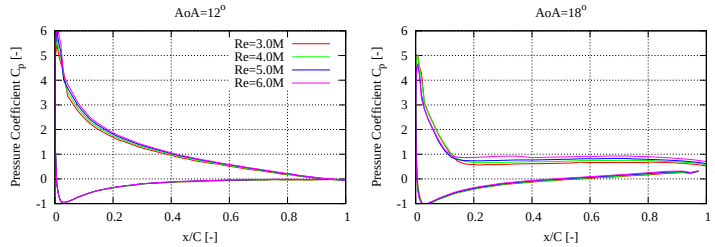

(a) NACA-0015

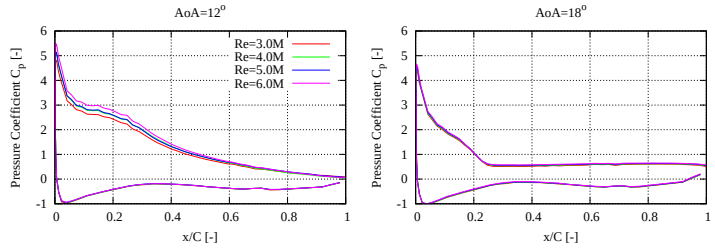

(b) RISØ-B1-18

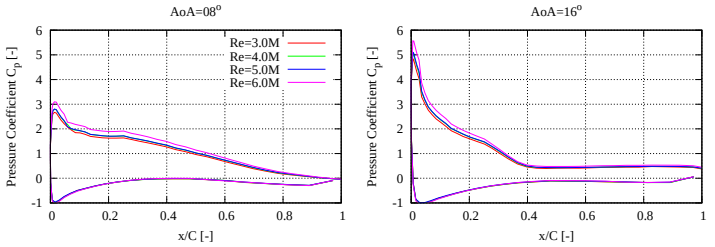

(c) NACA-63-418

Figure 3: Pressure coefficient distributions

recirculating flow region on the suction side of the airfoil. Within this separated recirculating flow, turbulent vortices are created and these vortical structures are eventually convected away into the airfoil wake. This occurs under the action of the ambient main flow passing around the airfoil and the recirculating region. The main flow exerts a downstream traction on the recirculating region through a mix of natural and turbulent momentum diffusion, which results in the turbulent stall vortices being carried away into the airfoil wake. As a result, the turbulent vortices can be roughly conceptualized as emerging near the separation point (location on the airfoil surface separating the upstream attached region of the flow and the recirculating zone downstream) and travelling along the airfoil chord at some specific speed. This convection velocity may vary from one vortical structure to another and might in some cases also be negative (i.e. a vortex may momentarily be travelling upstream) precisely because of the recirculating characteristics of the mean separated flow. However, statistically all vortices can be considered as travelling downstream.

As the separated flow is turbulent, it is inherently unsteady and the turbulent vortical structures vary randomly, but continuously, in time and space. Considering sufficiently small time intervals, it is usually valid to assume (Taylor's hypothesis) that the turbulence characteristics are frozen and that the turbulent vortices convect at a constant speed which is referred to as 'turbulence convection velocity', or 'convection velocity' for short.

Convection velocity can be calculated as follows. Using the signals from two microphones separated by a distance Δx along the chord, the cross-correlation function between the two time-series is computed. Then, the time difference $\Delta\tau_{\text{max}}$ at which this function reaches its maximum value is evaluated. It is clear that the surface pressure measured at the upstream microphone and generated by specific vortical structures will

be most correlated to the surface pressure measured at the downstream microphone and generated by the same structures as these have convected to this new location. Therefore, assuming frozen turbulence the convection velocity can be estimated by the simple formula:

$$U_{\mathsf{cv}} = \Delta x / \Delta \tau_{\mathsf{max}}$$

Note that this calculated convection velocity is actually not characterizing the speed of each individual vortex, but rather the speed at which their footprints as surface pressure fluctuations travel.

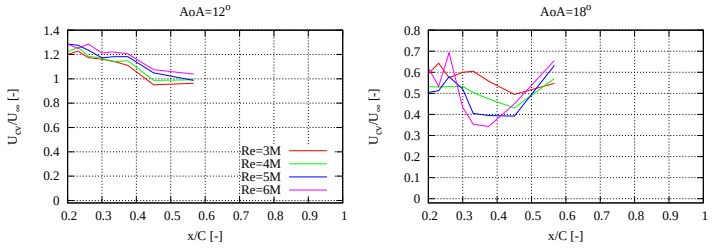

(a) NACA-0015

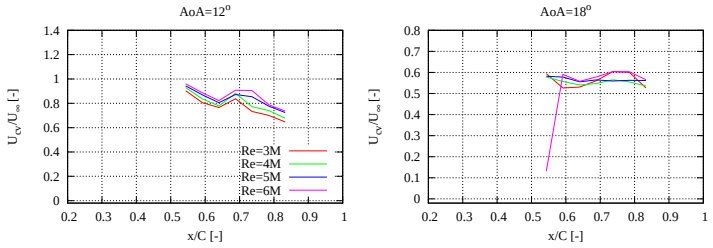

(b) RISØ-B1-18

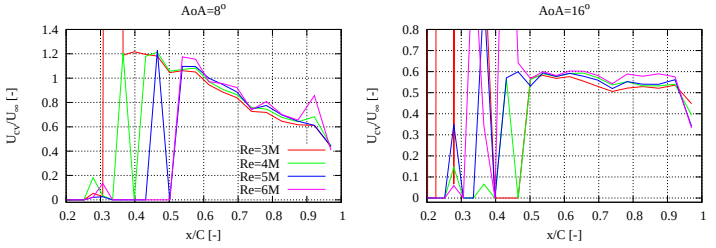

(c) NACA-63-418

Figure 4: Convective velocities U_{cv}

In Figs. 4(a-b-c), the convection velocities are plotted as a function of the downstream microphone position at the two angles of attack considered in the previous section for attached and stalled flow conditions. It can be seen here that the microphone distributions vary significantly for the different airfoils. The NACA-0015 airfoil has microphones located relatively close to the leading edge and only cover a small portion of the separated region in the stalled case, while for the RISØ-B1-18 airfoil they are located from the mid-chord to $x/C \approx 0.83$. However, in the case of the NACA-63-418 airfoil the microphones span almost along the entire chord. The figures clearly show that in the case of attached flow conditions, the convection velocity is larger than the inflow velocity near the leading edge, starting at values around $1.2 \times U_\infty$ for $x/C \approx 0.2$, and slowly decreases as the trailing edge is approached down to $U_{\mathsf{cv}} \approx 0.6 \times U_\infty$. In the case of stalled flow conditions, the normalized convection velocity is roughly constant in the separated region and varies between values ranging from 0.5 to 0.6 depending on the considered airfoil and the location along the airfoil chord.

As an approximation, the constant value $U_{\text{cv}}/U_\infty = 0.55$ will be assumed for the calculations performed in the remaining of this study. Though arbitrary, this choice should only have secondary effects on the results that will be displayed below.

5. Stochastic Characterization of Stall through Correlation Length

In addition to the convection velocity, an important quantity characterizing a turbulent flow field is the correlation length. In our case, the quantity of interest is the surface pressure and its correlation length both in the chordwise and spanwise directions. Unfortunately, the experiments considered in this article cannot provide any information about the spanwise correlation since microphones were not distributed along the span of the airfoil sections. Contrastingly, the correlation length in the chord direction can actually be estimated using a single microphone. Assuming frozen turbulence and that the turbulent fluctuations convect at the known convection velocity $U_{\text{cv}} = 0.55 \times U_\infty$ as specified above, the temporal auto-correlation function of the surface pressure time-series recorded by one microphone can be transformed into the auto-correlation of the same quantity as a function of separation length. Formally, it reads:

$$\begin{aligned} <u(x,t)\,u(x+y,t)> &= <u(x,t)\,u(x,t+y/U_{\text{cv}})> \\ &= f(\tau = y/U_{\text{cv}}) \equiv <u(x,t)\,u(x,t+\tau)> \end{aligned}$$

where the brackets $<...>$ denote ensemble averaging which can be achieved by assuming temporal homogeneity, calculating the auto-correlation functions centered at various instants t during the time-series, and averaging the resulting functions. x is the position of the microphone along the airfoil chord, y the separation length, and $f(\tau)$ is the calculated temporal auto-correlation function depending on the separation time τ. Assuming that the turbulent fluctuations convect parallel to the chord, the correlation length in the chord direction L_x is formally defined as:

$$L_x = \int_0^\infty \frac{<u(x,t)\,u(x+y,t)>}{<u(x,t)\,u(x,t)>}\,\mathrm{d}y = U_{\text{cv}} \cdot \int_0^\infty \frac{<u(x,t)\,u(x,t+\tau)>}{<u(x,t)\,u(x,t)>}\,\mathrm{d}\tau$$

The calculated correlation lengths are plotted in Figs. 5(a-b-c) for the two angles of attack considered in the previous sections. Note that these lengths have been normalized by the chord and multiplicated by the square root of the inflow velocity (see explanation below). It can be seen that the correlation lengths are much smaller for the attached flow conditions than for the stalled ones. This indicates that turbulent vortices present in the detached region are considerably larger than those present in the attached turbulent boundary layer, as it could be expected. In the detached cases, the correlation length grows linearly as a function of chord location toward the trailing edge and cancels at (or near) the separation point, which can be inferred from the pressure coefficient distributions plotted in Fig. 3 or from the present curves. However, in Fig. 5(a) the NACA-0015 airfoil displays peculiar behaviour at higher Reynolds numbers for which the correlation lengths grow very rapidly to high values before returning to more sensible ones at the most downstream microphone. This may be attributed to the fact that the microphones are located near the separation point, which seems to disrupt the numerical evaluation of the correlation length as illustrated in Fig. 5(c) by the oscillatory correlation lengths calculated near the separation point for the NACA-63-418 airfoil for $0.2 < x/C < 0.45$.

It is interesting to note that the slopes of the linear growth of the correlation length as a function of chord location almost coalesce, independently of airfoil and Reynolds

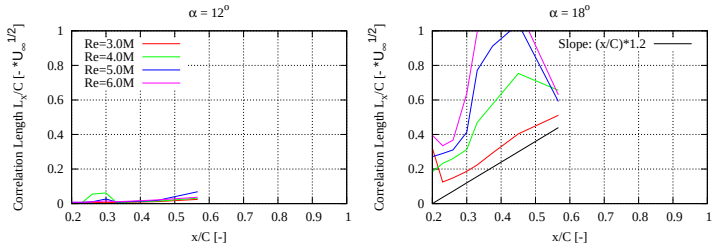

(a) NACA-0015

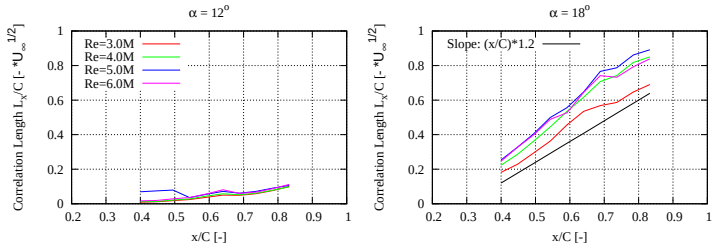

(b) RISØ-B1-18

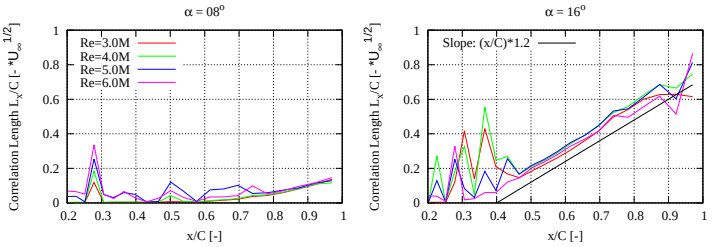

(c) NACA-63-418

Figure 5: Correlation lengths L_x in chord direction

number (except for the NACA-0015 airfoil at high Reynolds numbers as noted above), when using the $\sqrt{U_\infty}$ scaling for plotting this functions. The 1.2 slope factor seems to be nearly universal although the RISØ-B1-18 airfoil case exhibits slightly higher slopes for $Re \geq 4M$. The present correlation data will not be used in the following, however the above results indicate that any physical value which is a linear function of the distance from the separation point is related to the scaled correlation length and is therefore a good candidate for the scaling of averaged stochastic turbulent quantities (see next section).

6. Surface Pressure Spectral Characteristics of Stall and Scaling

In this section, the surface pressure spectra measured at different microphone locations and for different angles of attack are investigated. As shown in the previous sections, stall is characterized by turbulent vortices that have larger sizes than those generated in an attached turbulent boundary layer and they have smaller convection velocities. It is therefore expected that this should be reflected in the measured surface pressure spectra as stall occurs. This can indeed be observed in Fig. 6 which displays these spectra for the NACA-63-418 airfoil at angles of attack equal to $\alpha = 8, 12, 16^o$ and for microphones located at $x/C = 0.54, 0.74, 0.92$. For the lowest angle of attack (for which the flow is still attached) and at frequencies below approximately 1000 Hz, the spectra are relatively flat. However, when the angle of attack increases to 12^o, flow separation appears in the trailing edge region and the two microphones located in the separated region of the detached flow (at $x/C = 0.74$ and 0.92) exhibit high energy spectral humps centered between 100 and 200 Hz depending on the Reynolds number, whereas the microphone located in the attached region (at $x/C = 0.54$) still

exhibits a flat spectrum in this frequency range. At the highest angle of attack, all three microphones are located in the separated region and all exhibit high energy spectral humps however centered toward lower frequencies compared to the previous angle of attack. Similar observations can be made with the two other airfoils but these plots are not shown here for the sake of brevity.

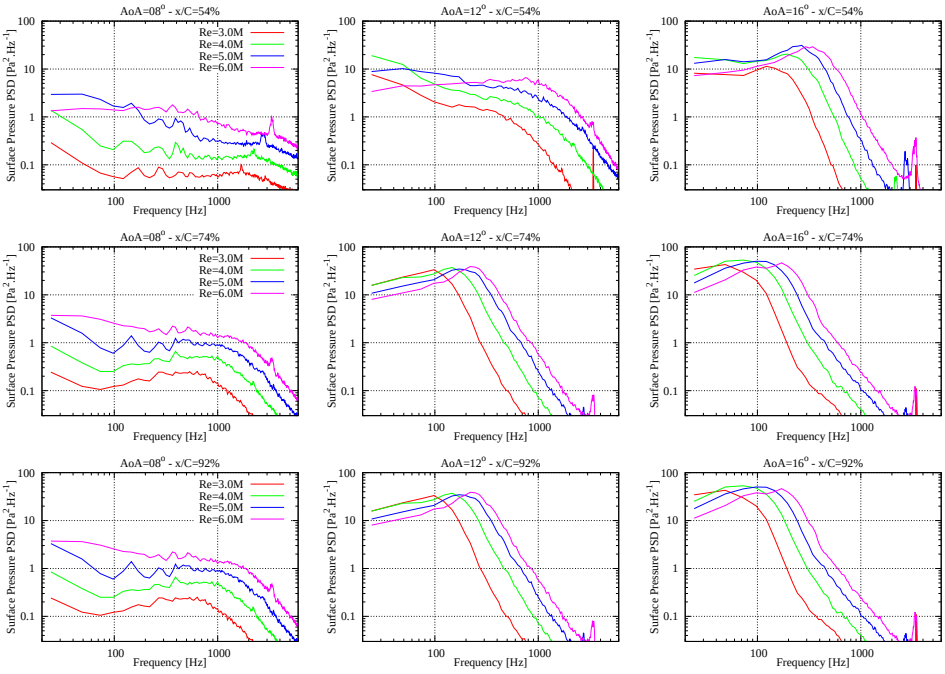

Figure 6: Surface pressure spectra for the NACA-63-418 airfoil

In an attempt to unify the effect of stall on the surface pressure spectra measured by the microphones located in the separated region, the spectra are non-dimensionalized as follows. Firstly, the separation point locations x_{sep} on the airfoil suction sides are located using the pressure coefficient distributions for each angle of attack, each Reynolds number and each airfoil. Thus, the distance L_{sx} of each individual microphone location to the separation point can be evaluated as: $L_{\text{sx}} = x_{\text{mic}} - x_{\text{sep}}$, where x_{mic} is the microphone location. The frequency f is then non-dimensionalized as a Strouhal number S_t using the above-defined distance and the inflow velocity as:

$$S_t = f \cdot L_{\text{sx}} / U_\infty$$

Secondly, the surface pressure power spectral density S_{pp} is non-dimensionalized using the inflow dynamic pressure and the normalized spectral bandwidth, and scaled with the Reynolds number as:

$$S_{\text{norm}} = S_{pp} \,/\, \left((0.5\,\rho\,U_\infty^2)^2 \cdot (L_{\text{sx}}/U_\infty) \cdot Re^{-5/2} \right)$$

The corresponding measured normalized spectra are plotted in Figs. 7(a-b-c) for the three airfoils at the two highest angles of attack for which the flow has stalled. It can be seen that the chosen scaling yields a reasonable collapse of the different spectral humps for the different microphone locations, angles of attack, Reynolds numbers, and for all airfoils. However, it should be noted that the NACA-0015 airfoil exhibits poor agreement with the other airfoils for the two most upstream microphones, but this may be linked to the peculiar behavior of the turbulence correlation lengths observed in

Section 5. The reasons for the observed discrepancies between the different normalized spectra may originate from an inadequate scaling (it must be reminded here that the chosen scaling is purely empirical and thereby arbitrary) and/or from the fact that the quantity L_{sx} used in the scaling may not have been accurately estimated from the measurement data.

Though not perfect, this collapse allows us to design a somewhat universal model for the surface pressure spectra in the frequency range characteristics of stall as described above, which approximately stretches in term of Strouhal number over the interval $0.1 < S_t < 2$. The following function is chosen as a global fit for the different measured and normalized spectra:

$$S_{\mathrm{model}}(S_t) = 0.8 \times 10^{13} \cdot S_t / (0.06 + S_t^4)$$

and it is plotted in the figures for comparison. Though not fully universal, this function is an acceptable approximation of the surface pressure spectra and can be used to estimate these spectra assuming that the parameters used for the normalization are known for a given airfoil.

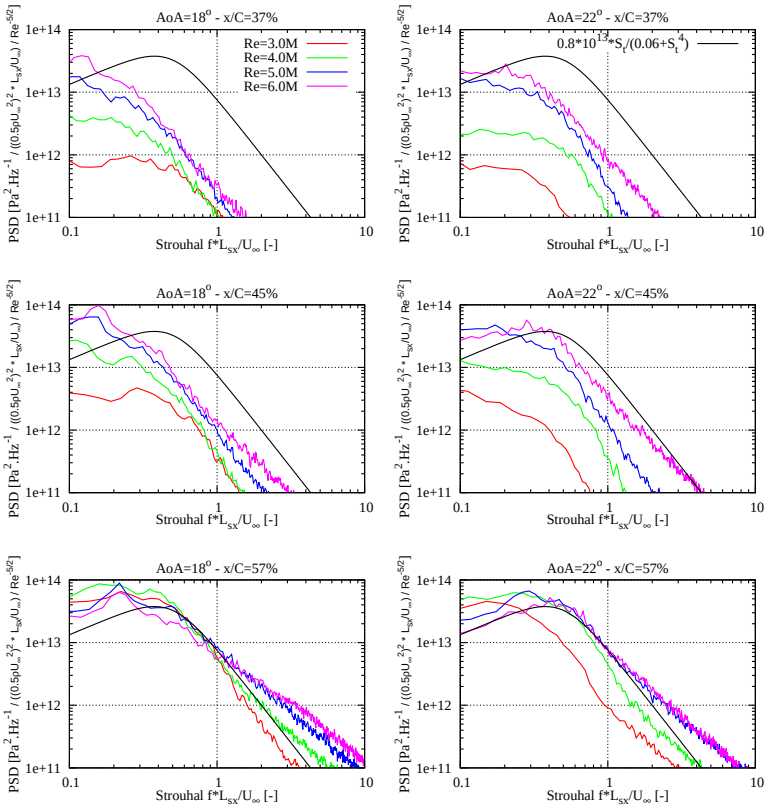

(a) NACA-0015

Figure 7: Normalized surface pressure spectra (Continuing below)

7. Discussion and Future Work

In this work, it was shown that the occurence of stall has a very characteristic effect on the surface pressure spectra measured in the separated region of the flow, which amounts to the emergence of a spectral hump at low frequency. A specific normalization and scaling of the spectra yields a roughly universal model for these spectra in this frequency range, though this model may require some further refinements to become more general.

The final objective of this study is the modelisation of stall noise. In a previous paper by Moreau et al. (2009), a model was proposed. It uses a distribution of equivalent dipole acoustic sources along the airfoil surface to simulate the effect of the stall vortices. The intensity of the dipoles were set in accordance with the surface pressure spectra measured with microphones flush-mounted on the airfoil in a manner similar to the present work. This model showed good agreement with the far-field noise that was also measured during their experiment.

In our case, the goal is to devise a model that doesn't require any measurement data but only the knowledge of the flow quantities specified above to perform the normalization. In the next step of this study, the proposed universal spectrum will be used to specify the surface pressure spectra and thereby the dipole intensites. The flow quantity used for the normalization can be evaluated with an airfoil flow solver such as Xfoil or a CFD code.

Acknowledgements

Authors would like to acknowledge the support of the Danish Energy Agency (Energistyrelen) that funded the DANAERO MW and DANAERO MW II projects (Contract nos. ENS-33033-0074 and ENS-64009-0258).

The authors are very thankful to LM Wind Power for allowing access to their wind tunnel.

The authors would also like to thank Brüel & Kjær Sound & Vibration Measurement, in particular Anders Eriksen and Rémi Guastavino, for their help in developing the high-frequency microphones measurement system and its calibration.

References

Fischer, A., Bertagnolio, F., Bak, C., & Madsen, H. A. (2010). Surface Pressure Measurements on a NACA0015 Airfoil Compared to Computations with the TNO Trailing Edge Noise Model. In *Torque 2010 'The science of making torque from wind' Conference (EWEA)*, Conf. Proceedings, (pp. 81–92). Heraklion, GR.

Guastavino, R. (2010). On-site Microphone Calibration for 'Low Noise Airfoil' EUDP Project J.nr. 64009-0272. Tech. Rep. (Private Communication), Brüel & Kjær Sound & Vibration Measurement A/S, Nærum, Denmark.

Madsen, H. A., Bak, C., Paulsen, U. S., Gaunaa, M., Fuglsang, P., Romblad, J., Olesen, N. A., Enevoldsen, P., Laursen, J., & Jensen, L. (2010). The DAN-AERO MW Experiments - Final report. Tech. Rep. Risø-R-1726(EN), Risø-DTU, Roskilde, Denmark.

Madsen, H. A., Bertagnolio, F., Andreas, A., & Bak, C. (2014). Correlation of Amplitude Modulation to Inflow Characteristics. In *Internoise 2014*, Conference Proceedings. Melbourne, Australia.

Moreau, S., Roger, M., & Christophe, J. (2009). Flow Features and Self-Noise of Airfoils Near Stall or Stall. In *Proc. of the* 15^{th} *AIAA/CEAS Aeroacoustics Conf.*, AIAA Paper 2009-3198. Miami, FL.

Smith, M., Bullmore, A. J., Cand, M. M., & Davis, R. (2012). Mechanisms of Amplitude Modulation in Wind Turbine Noise. In *Acoustics 2012*, Conference Proceedings. Nantes, France.

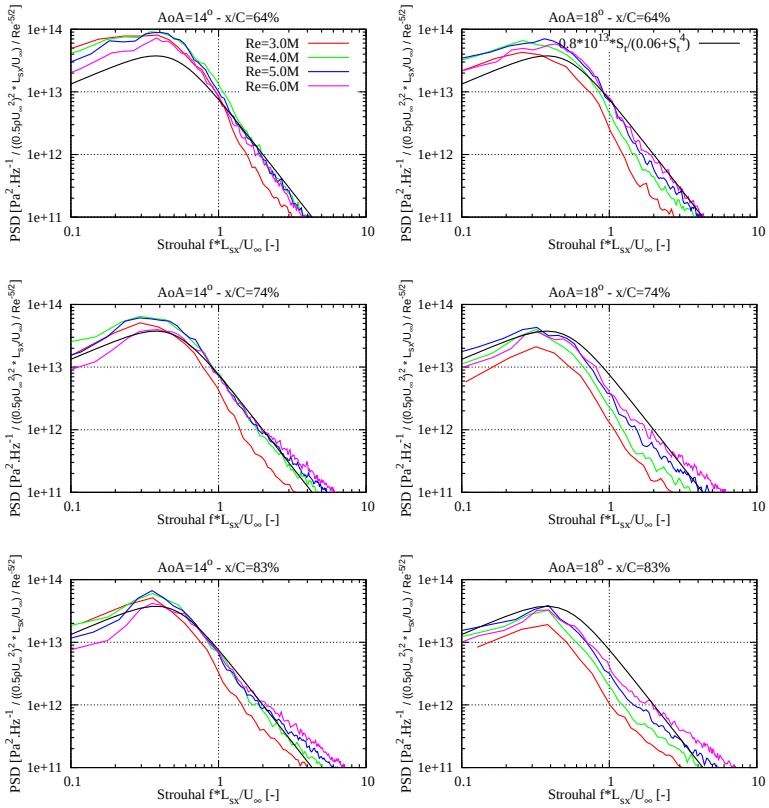

(b) RISØ-B1-18

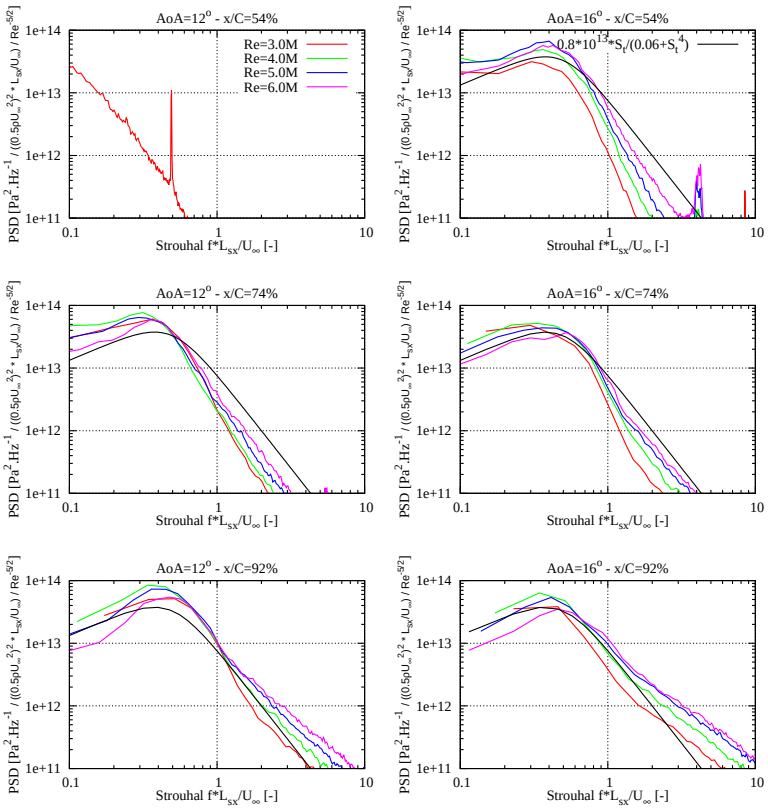

(c) NACA-63-418

Figure 7: Normalized surface pressure spectra (Continued)